Applied Surface Science 702 (2025) 163383

Contents lists available at ScienceDirect

Applied Surface Science

journal homepage: www.elsevier.com/locate/apsusc

Full Length Article

Effect of alpha olefins as additives on the friction performance of a-C/PAO composite systems under variable load conditions

Jiahao Dong [a], Naizhou Du [a], Xubing Wei [a], Xiang Ji [b,*], Xuanru Ren [b], Peng Guo [c], Rende Chen [a], Jie Wu [d], Lei Wang [d], Haibin He [d], Kwang-Ryeol Lee [e], Aiying Wang [c,*], Xiaowei Li [a,c,*]

[a] School of Materials Science and Physics, China University of Mining and Technology, Xuzhou 221116, PR China
[b] Henan Key Laboratory of High Performance Carbon Fiber Reinforced Composites, Institute of Carbon Matrix Composites, Henan Academy of Sciences, Zhengzhou 450046, PR China
[c] State Key Laboratory of Advanced Marine Materials, Ningbo Institute of Materials Technology and Engineering, Chinese Academy of Sciences, Ningbo 315201, PR China
[d] Ningbo C.S.I. Power & Machinery Group Co., Ltd., Ningbo 315020, PR China
[e] Computational Science Center, Korea Institute of Science and Technology, Seoul 136-791, Republic of Korea

ARTICLE INFO

Keywords:
Amorphous carbon
Lubricant additives
Fluid dynamic lubrication
Interface passivation
Reactive molecular dynamics

ABSTRACT

The tribological performance of amorphous carbon (a-C) and PAO oil composites is critical for mechanical system. However, the impact of unsaturated AO molecules in PAO oil on the a-C/PAO system under variable loads complicating experimental characterization and understanding of friction mechanisms. Herein, reactive molecular dynamics simulations were employed to systematically examine the influence of AO molecules on the friction behavior of a-C/PAO composite systems under variable load conditions. Results reveal distinct pressure-dependent mechanisms governing the tribological behavior, highlighting the interplay between hydrodynamic lubrication and interfacial passivation. At low contact pressure, friction behavior is primarily governed by hydrodynamic lubrication, where an increase in AO chain length reduces lubricant mobility. Upon increasing contact pressure to 50 GPa, the friction interface transitions to a regime dominated by the competitive interplay between hydrocarbon passivation and C–C bond formation, but the degree of interfacial passivation induced by AO molecules results in variations in friction performance. As pressure further reverts to 5 from 50 GPa, the fracture of long-chain AO molecules into shorter fragments weakens the difference in interfacial structures between systems. These results deepen the understanding of friction mechanisms involving AO molecules in a-C/PAO systems and provide theoretical guidance for designing high-performance lubrication systems.

1. Introduction

Friction and wear have become increasingly critical issues in mechanical systems, with friction-related energy consumption accounting for approximately 23 %[1] of global energy use annually. Therefore, the development of efficient lubrication systems is essential for enhancing energy efficiency and extending the service life of key components. Amorphous carbon (a-C) films have garnered significant attention as solid lubricating materials due to their high hardness, low friction coefficient, and excellent wear resistance[2–4]. Integrating these films with fluid lubricants (PAO, et al.) to form solid–liquid composite lubrication systems can effectively mitigate the self-consumption of a-C films while significantly enhancing the service life and wear resistance of mechanical components[5–8].

Fluid lubricants typically consist of a base oil and various nanomaterial additives. Dispersed within the base oil, these additives not only stabilize the lubricant but also enhance the overall performance of solid–liquid lubrication systems, making them indispensable for engineering and technical applications[9,10]. Commonly used lubricant additives, such as molybdenum dithiocarbamate (MoDTC)[11–14] and zinc dialkyl dithiophosphate (ZDDP)[15–18] play a crucial role in improving lubricant performance. These additives enhance the chemical stability and antioxidant properties of the lubricant while significantly increasing its wear resistance and extreme pressure capabilities[19,20]. Liu's study[21] investigated the effect of temperature and the friction pair on the interaction between a-C films and lubricant additives under

* Corresponding authors.
E-mail addresses: jixiang_manuscript@163.com (X. Ji), aywang@nimte.ac.cn (A. Wang), lixw0826@gmail.com, xwli@cumt.edu.cn (X. Li).

https://doi.org/10.1016/j.apsusc.2025.163383
Received 2 April 2025; Accepted 25 April 2025
Available online 26 April 2025

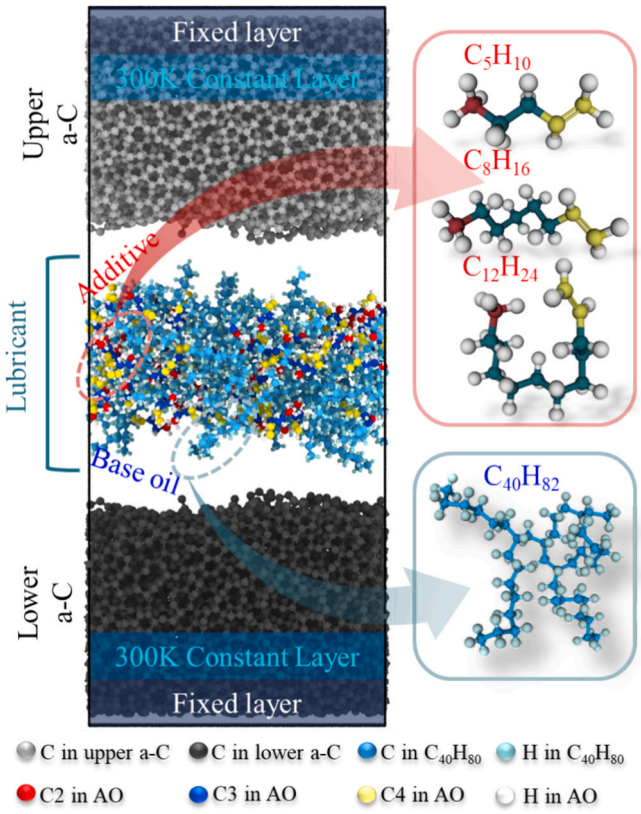

Fig. 1. Simulated model for a-C/lubricant/a-C.

high Hertzian contact stresses. The results showed that adding MoDTC additive at high temperature could reduce the friction coefficient of steel mating pairs to half of pure base oil, but significantly increase the friction coefficient of self-mating pairs. While the addition of ZDDP slightly reduced the friction coefficient, the overall performance remains suboptimal. This is different from the findings under low Hertzian contact stress[22]. Furthermore, according to Tokoroyama's findings[23], the friction-reducing efficacy of MoDTC diminished with increasing load for ta-C films characterized by lower hardness. Therefore, it is essential to explore lubricant additives that can effectively cope with complex working conditions, especially high-pressure working conditions.

In particular, PAO base oil as a lubricant has been widely used in the high-tech fields of automobile, aerospace and so on due to its physicochemical properties. However, during the synthesis process of PAO oil, there is the inevitable existence or residual of unsaturated alpha-olefin (AO) molecules, which exhibit excellent lubricating properties due to their unique molecular structure. The presence of double bonds in their structure makes AO prone to cleavage under high-pressure conditions. During the sliding process, the resulting hydrocarbon fragments effectively passivate the dangling bonds on the a-C surface, thereby significantly enhancing the tribological performance of a-C films[24]. Through molecular dynamics simulations, Li[25] demonstrated that the introduction of AO molecules into the a-C interface could maintain a low friction coefficient even under extremely high-pressure conditions of 50 GPa.

The above-mentioned finding implies the potential selection of AO molecules as lubricant additives for enhancing the anti-friction performance of composite system. However, in the a-C/PAO composite system, the effect of AO molecules as additives on friction behavior is still lack of study. In addition, dynamic machinery often faces variable load conditions during operation, and the mechanism of performance changes in solid–liquid composite systems under such variable load conditions is still unclear. Meanwhile, the introduction of PAO and AO molecules and the complicated a-C structure transformation further aggravate the difficulty in accurately characterizing the friction interface from experiment[26,27], which is a big challenge for explaining the lubrication mechanism from a macroscopic experimental perspective. In order to effectively understand the role of AO molecules and guide the design of a-C/PAO composite systems, in-situ exploration at the atomic scale is required to reveal the structural evolution and dynamic friction behavior of the friction interface.

In this study, the friction behavior of a-C/PAO composite systems under variable load conditions was investigated through reactive molecular dynamics (RMD) simulation. The effects of AO type and variable load on friction behavior were systematically evaluated by selecting $C_{40}H_{82}$ as the PAO base oil while linear AO with varying chain lengths (C_5H_{10}, C_8H_{16}, and $C_{12}H_{24}$) were employed as lubricant additives. Additionally, the study comprehensively examined the evolution of interfacial structures, the interactions among AO, $C_{40}H_{82}$, and a-C, as well as the flow behavior of fluid lubricants, to elucidate the synergistic lubrication mechanism. The findings demonstrate that incorporated AO as a lubricant additive significantly enhances the structural stability of base oil under variable load conditions. This study provides an important theoretical basis for the optimization design of fluid lubricants.

2. Methods

The molecular dynamics simulations (MD) mentioned in this study were conducted in Large-scale atomic/molecular massively parallel simulators (LAMMPS)[28]. As shown in Fig. 1, the model consisted of three parts: lower a-C, lubricant (containing 20 $C_{40}H_{82}$ molecules and linear AO molecules of varying chain lengths as additives), and upper a-C. The initial a-C structure was generated through atom-by-atom deposition simulations[29]. According to the different lubricant additives, the dimensions of the models were: 42.88 × 40.358 × 97.2877 $Å^3$, 42.88 × 40.358 × 103.0615 $Å^3$, 42.88 × 40.358 × 104.2544 $Å^3$, 42.88 × 40.358 × 103.9130 $Å^3$, named separately as a-C/$C_{40}H_{82}$/a-C, a-C/$C_{40}H_{82}$ + C_5H_{10}/a-C, a-C/$C_{40}H_{82}$ + C_8H_{16}/a-C, and a-C/$C_{40}H_{82}$ + $C_{12}H_{24}$/a-C. In addition, to distinguish between pure base oil systems and systems with added additives, the pure base oil system is named a-C/PAO/a-C, and the systems with added AO are named a-C/PAO + AO/a-C.

Before friction simulations, each system was functionally divided into three layers: the fixed layer, the thermostat layer, and the free layer. The fixed layer, designed to simulate a semi-infinite system, consisted of the lower a-C substrate and the upper a-C counterface, each with a thickness of 5 Å. (dark blue regions in Fig. 1); The thermostat layer was adjacent to the fixed layer with a thickness of 5 Å (shown in light blue in Fig. 1), used the Berendsen[30] thermostat within the NVE ensemble to maintain a temperature of 300 K; The free layer was composed of the remaining a-C, base oil, and additives, used to simulate the structural changes caused by friction at the interface. The simulation employed a time step of 0.25 fs, with periodic boundary conditions applied along the x and y axes. The ReaxFF potential was used to describe the C–C, C–H, and H-H interactions throughout the system[31]. Its accuracy has been validated in our previous work[32–34].

During the friction simulation, the entire system was first relaxed at 300 K for 2.5 ps. Subsequently, the upper a-C layer was loaded to the specified contact pressure of 5 GPa along the z-axis within 25 ps. The fixed layer of the upper a-C film was then slid at a constant speed of 10 m/s along the x-axis for 1750 ps. Ma[35,36] found that the instantaneous contact pressure of the asperities on the a-C surface could reach up to 50 GPa during the friction process. Additionally, previous studies have also demonstrated that investigating the tribological performance of the a-C/fluids lubricant composite system under 50 GPa is reasonable [25,37]. Therefore, the entire sliding process was divided into three stages: first, sliding at a low pressure of 5 GPa for 500 ps (Stage I); followed by sliding for 250 ps under an extremely high pressure of 50 GPa (Stage II); and finally, returning to a low pressure of 5 GPa for 1000 ps (Stage III). The pressure transition from 5 GPa to 50 GPa occurred during

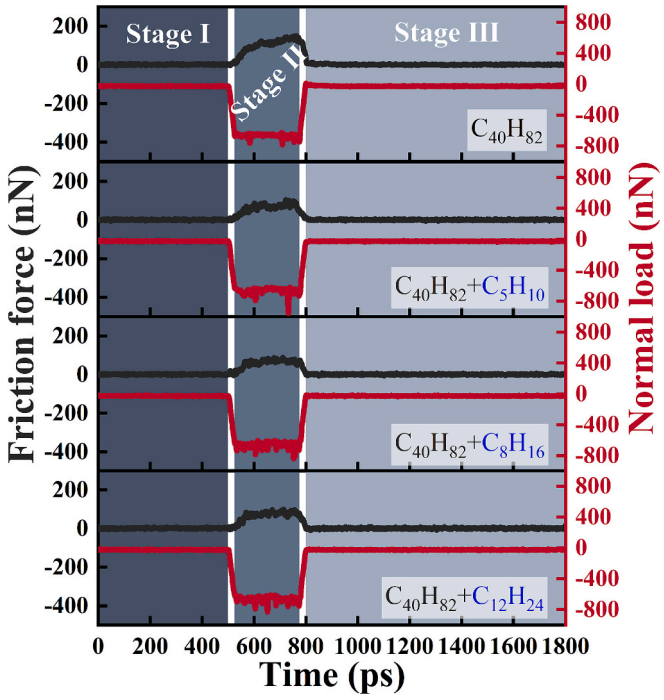

Fig. 2. Friction force and normal curves with the sliding time of each system.

500–525 ps, while the unloading from 50 GPa to 5 GPa took place during 775–800 ps. This setup simulated the friction behavior of the system under variable loading conditions.

3. Results and discussion

Fig. 2 illustrates the variations in friction force and normal load over sliding time for each system. In Stage I, the friction curves are smooth and stable, without a discernible running-in phase. This stability is attributed to the lubricant's ability to separate the upper and lower a-C layers under low pressure, preventing direct contact at the interface; In Stage II, as the contact pressure rises to 50 GPa, the friction force increases significantly, and the friction curve exhibits violent fluctuations, reflecting strong chemical interactions at the friction interface. These fluctuations are similar to the intense energy release processes observed in intrinsic a-C bonding under dry or mixed lubrication conditions[38], indicating that under high-pressure conditions, the interfacial friction mechanism may gradually shift from lubrication-dominated to a-C interaction dominated; In Stage III, when the pressure decreases back to 5 GPa, the friction curve stabilizes and returns to a smooth state similar to that in Stage I, indicating that at lower pressure, the lubricant can once again function effectively, reducing direct contact at the friction interface and re-establishing a favorable lubrication state.

The average friction force, normal load, temperature, and real contact area of different systems are quantified over the last 200 ps of each stage based on Fig. 2 (Fig.S1, Support Information). As shown in Fig.S1, for the a-C/$C_{40}H_{82}$/a-C system, the average friction force decreases after exposure to high pressure, which is attributed to the passivation of dangling bonds at the friction interface. The introduction of AO into the base oil significantly reduces the average friction force of the system. However, as the chain length of the AO increases, there is a corresponding rise in the average friction force. In addition, under high-pressure conditions, the introduction of AO substantially lowers the temperature of the free layer, further indicating that AO can suppress the intense chemical interactions at the frictional interface, thereby reducing the overall energy dissipation of the system.

To quantify the influence of AO on friction performance, the friction coefficient (μ) is calculated according to formula (1) [32]:

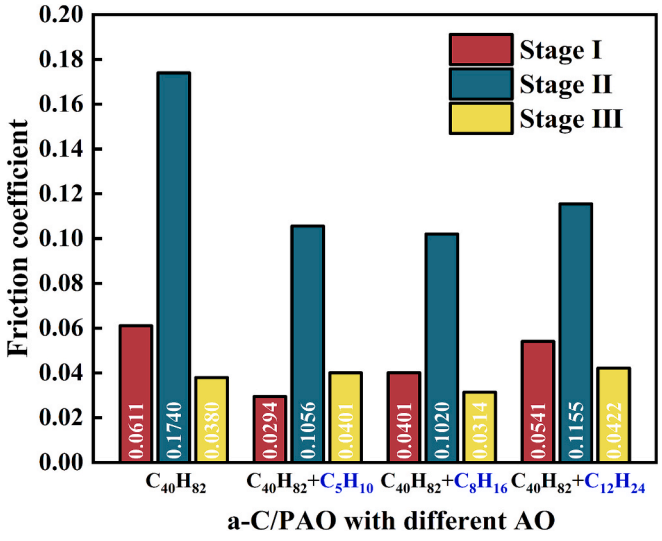

Fig. 3. Friction coefficient of each system.

$$\mu = \frac{f}{w} \tag{1}$$

where f is the friction force and w is the normal load, both taken from the last 200 ps of the stable stage shown in Fig. 2. As illustrated in Fig. 3, during Stage I, the isolating effect of the lubricant keeps the friction interface stable. The introduction of AO further reduces the friction coefficient, but as the AO chain length increases, the friction coefficient increases. This phenomenon can be attributed to the impact of longer-chain AO on the fluidity of the base oil. In Stage II, the sharp increase in contact pressure leads to a significant rise in the friction coefficient. During this stage, the friction interface undergoes substantial structural reorganization. Similar to Stage I, the friction coefficient shows a chain-length-dependent trend, suggesting that AO plays a crucial role in tribochemical reactions, particularly under high-pressure conditions where chain length significantly influences interfacial reactions. During Stage III, as the contact pressure decreases, the friction interface tends to stabilize, and the friction coefficient drops markedly compared to Stage II. However, following the interface structure reorganization under high pressure, the dependence of the friction coefficient on AO chain length becomes weakened. This may be due to intense tribochemical reactions that homogenize the interfacial structure, thereby diminishing the impact of chain length on friction behavior.

Notably, direct comparison between simulations and experiments remains significantly challenging due to: (i) the simplified friction models employed, (ii) discrepancies in tribological testing conditions, and (iii) the inherent difficulties in precisely controlling the molecular architectures of PAO/AO and the surface characteristics of a-C films (including roughness, dangling bond density, and surface contamination). Nevertheless, our simulation results demonstrate good agreement with experimental observations under comparable testing conditions [39,40].

To investigate the underlying mechanism behind the tribological performance changes of the a-C/PAO + AO/a-C system, the morphological characteristics of the system at different stages are analyzed, with the system without AO as a comparison (a-C/PAO/a-C system, Fig. 4a). Fig. 4 shows the interfacial morphology at the end of each sliding stage.

In Stage I, the lubricant is uniformly distributed across the friction interface, effectively isolating the upper and lower a-C surfaces and preventing them from having direct contact. However, after introducing AO, the distribution of lubricant became regionalized (Fig. 4b, Fig.S2). By excluding the atomic trajectories of the base oil (Fig. 4c), it can be

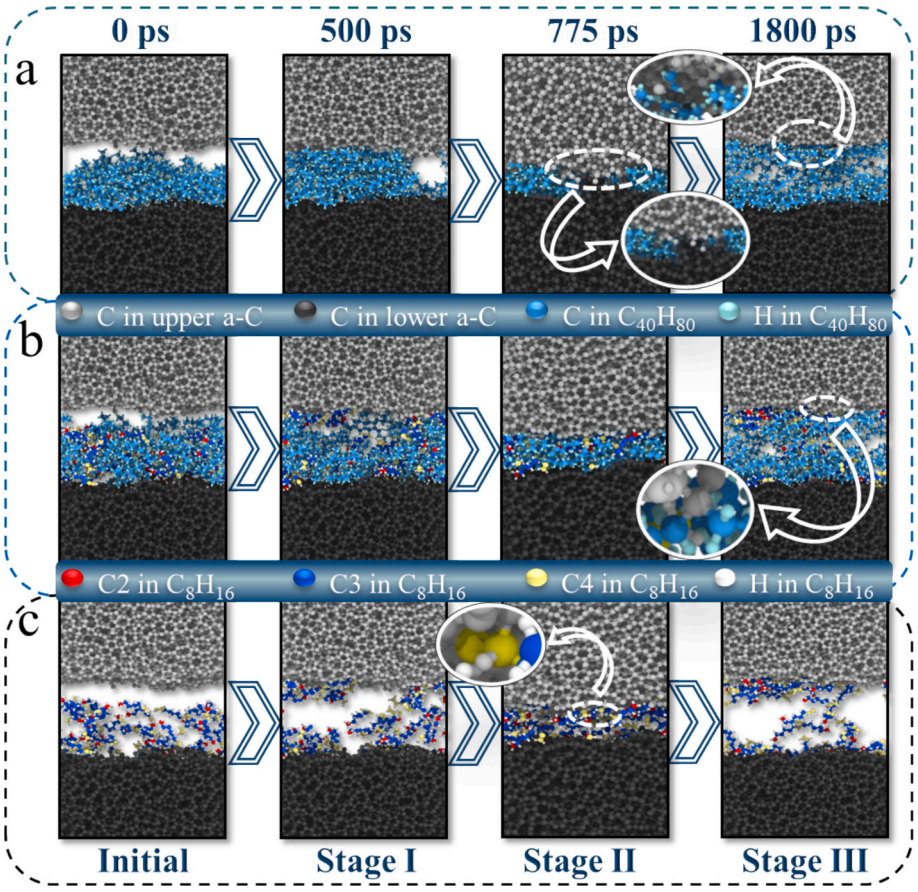

Fig. 4. Evolutions of interfacial morphologies of a) a-C/$C_{40}H_{82}$/a-C system, b) the overall a-C/$C_{40}H_{82}$ + C_8H_{16}/a-C system, and c) the a-C/$C_{40}H_{82}$ + C_8H_{16}/a-C system without $C_{40}H_{82}$. Other a-C/PAO + AO/a-C systems are shown in supporting information.

observed that AO tends to preferentially adsorb onto the a-C surface, causing an uneven distribution of base oil molecules at the interface. This adsorption effect likely arises from the strong interactions between the molecular structure of AO and the a-C surface, altering the macroscopic distribution characteristics of the lubricant.

In Stage II, significant direct contact is observed between the upper and lower a-C surfaces in the a-C/$C_{40}H_{82}$/a-C system due to high pressure, indicating the isolation effect of the lubricant has failed. However, in the a-C/$C_{40}H_{82}$ + C_8H_{16}/a-C system, the introduction of AO effectively enhances the load-bearing capacity of the base oil, and no obvious C–C bondings occur at the friction interface (Fig. 4b), suggesting that the addition of AO molecules could help maintain fluid lubrication and reduce solid–solid contact. Notably, under extremely high pressure at 50 GPa, base oil and AO molecules not only adsorb onto the a-C surface through intermolecular interactions but some molecules also undergo shear-induced cleavage, forming hydrocarbon fragments that chemically bond with surface atoms of a-C (Fig. 4c). These hydrocarbon molecules occupy the active sites on the a-C surface, gradually saturating the surface carbon atoms.

In Stage III, due to the bonding of some hydrocarbon molecules with the a-C surface and the presence of dangling bonds, the lubricant molecules tend to adsorb more strongly onto the a-C surface, with the distribution of the lubricant becoming more sparse compared to Stage I. This change in distribution reflects that the interfacial structural reconstruction after high-pressure treatment has affected the lubricant's adsorption behavior and flow characteristics. During this stage, the friction interface exhibits a coexistence of hydrodynamic lubrication and surface passivation effects.

The fracture and re-bonding behavior of base oil and AO molecules under high-pressure conditions significantly affect the hybridization

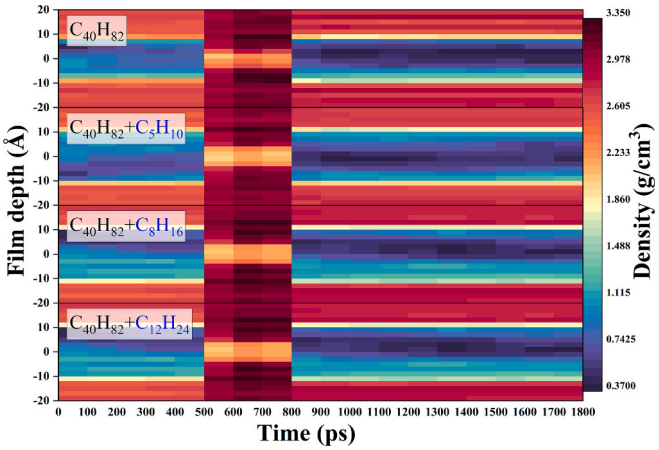

Fig. 5. Density distributions along the z-direction during the sliding process.

evolution of a-C at the friction interface. Especially the saturation tendency of surface carbon atoms can significantly improve the tribological performance of a-C films. However, in order to study the evolution of hybrid structures at the friction interface, it is necessary to first define the effective interface width to exclude interference from deeper a-C regions, which remain largely unchanged during the friction process.

Fig. 5 shows the mass density distribution along the z-direction. For each system, the friction system is divided into three regions: the lower a-C region, the interfacial region, and the upper a-C region. According to previous research[41], the interfacial width varies significantly under high and low pressure conditions. Therefore, the interfacial width is

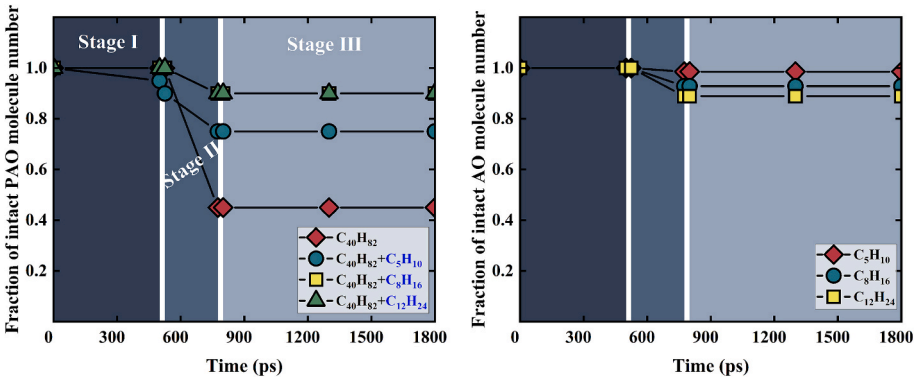

Fig. 6. Fraction of intact lubricant molecules during the sliding process. a) the PAO($C_{40}H_{82}$) molecules and b) the AO(C_5H_{10}, C_8H_{16} and $C_{12}H_{24}$) molecules.

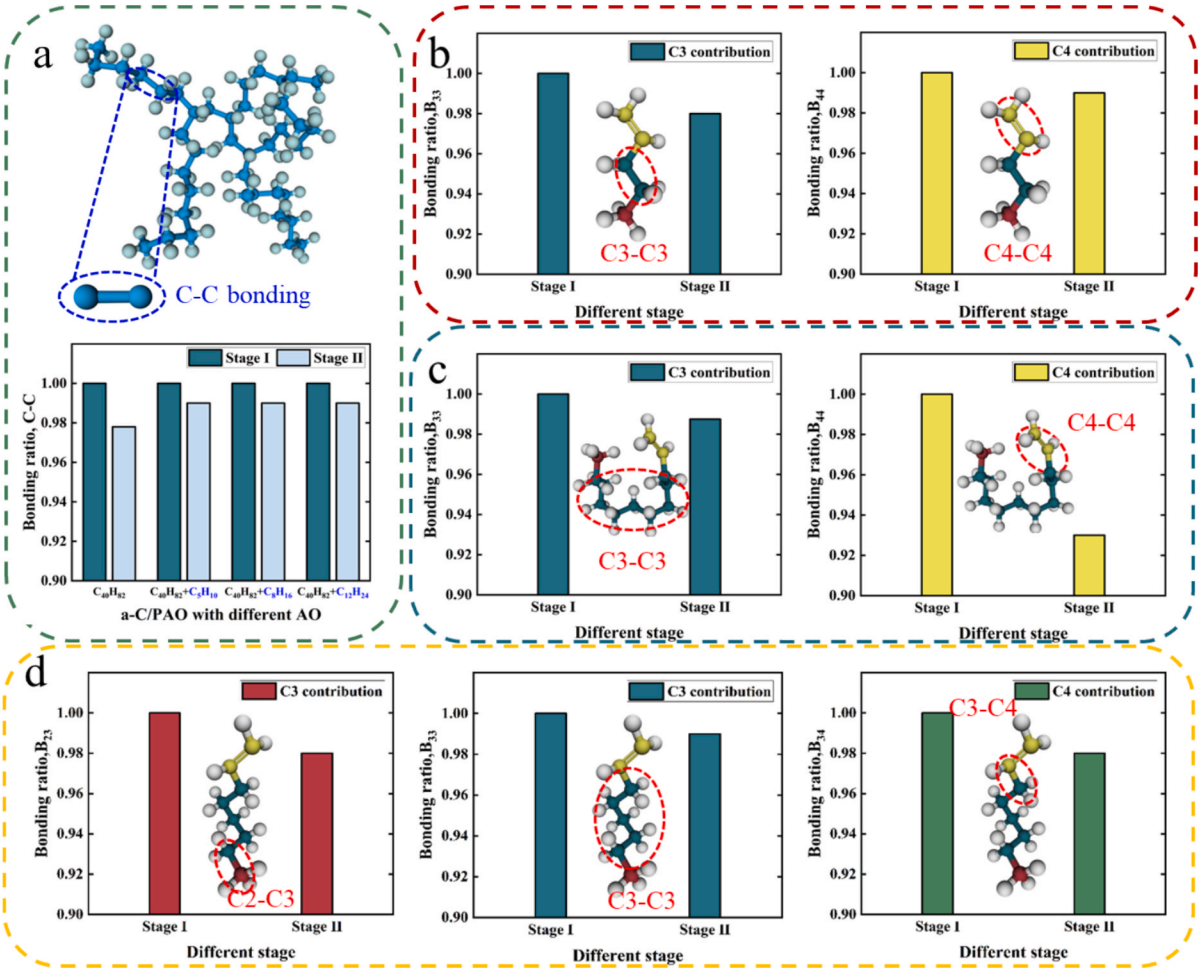

Fig. 7. A) c–C bondings of $C_{40}H_{82}$ molecules for each system. And bonding ratios between the C2, C3, and C4 atoms of b)C_5H_{10} molecules, c) $C_{12}H_{24}$ molecules, and d) C_8H_{16} molecules.

defined separately for these conditions. During Stage I, at a low pressure of 5 GPa, the structural evolutions are primarily concentrated in the interfacial region, indicating that the physical and chemical changes induced by friction are mainly confined to the frictional contact area between the upper and lower a-C surfaces. When the pressure increases to 50 GPa, strong interactions occur at the friction interface, leading to a significant increase in system density and substantial structural changes in the interface. Notably, when the pressure decreases to 5 GPa, the system density is lower than that in Stage I. This phenomenon can be attributed to the fracture behavior of the base oil molecules and AO molecules. During sliding under extreme pressure, these molecules may undergo structural decomposition or chemical bonding, with some molecules forming stable chemical bonds with the a-C surface while others are broken by shear forces. As the pressure decreases, the intermolecular interactions weaken, allowing some molecules to regain mobility, resulting in a decrease in the overall system density. The interfacial width does not show significant differences across AO molecules with varying chain lengths.

To determine the contribution of lubricant re-bonding behavior to the hybridization structure of a-C at the friction interface, Fig. 6a

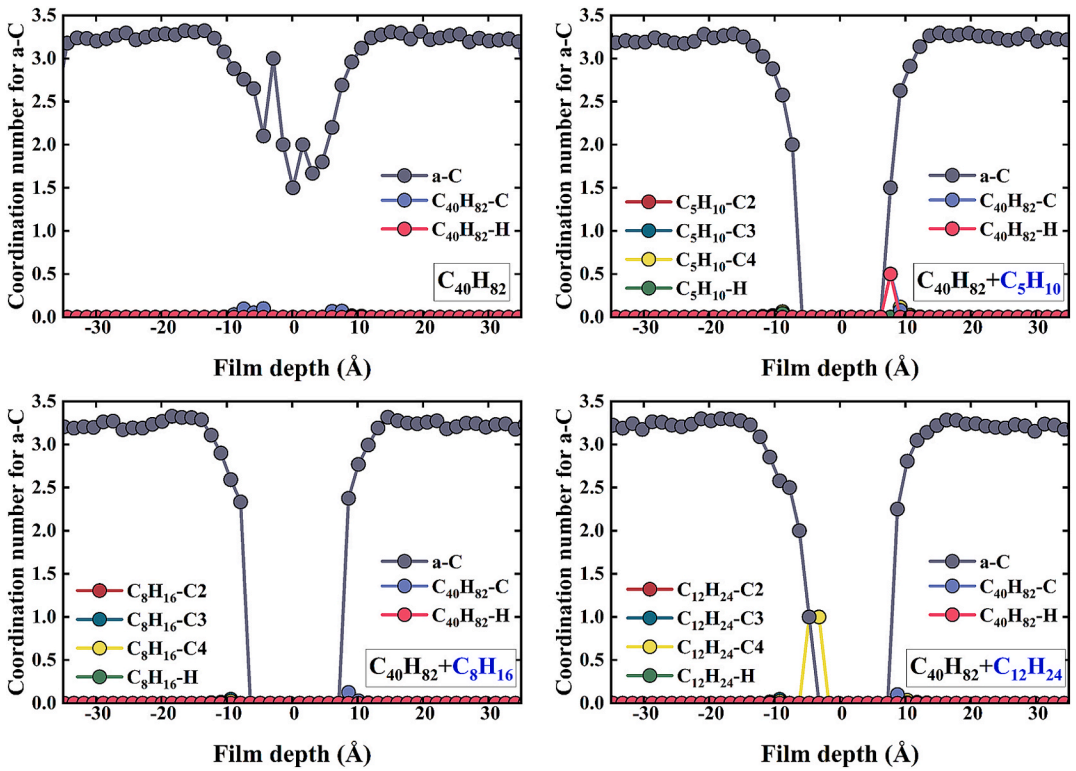

Fig. 8. Coordination number distribution of C atoms for the a-C structure.

presents the proportion of intact $C_{40}H_{82}$ molecules at each stage. During Stage I, there is no fracture phenomenon observed due to the weak interaction experienced by $C_{40}H_{82}$ molecules. At this stage, the isolating effect of the lubricant is effective, and the molecular interactions at the friction interface are limited. When the pressure increases to 50 GPa, a noticeable fracture of $C_{40}H_{82}$ molecules is observed, with only 45 % remaining intact. This is attributed to the strong shear forces and thermal effects exerted on the molecular chains of the base oil under extreme pressure. In Stage III, as the pressure decreases back to 5 GPa, the number of intact $C_{40}H_{82}$ molecules remains stable, and no further fracture phenomena are observed.

In addition, the breaking behavior of AO molecules at different stages is similar to that of base oil molecules (Fig. 6b). It is worth noting that as the length of the AO chain increases, the number of broken AO molecules also increases. This indicates that although long-chain AO molecules can provide stronger protection, their longer molecular chains are more susceptible to shear-induced damage under extremely high pressure conditions, leading to breakage.

To further identify the fracture sites of the base oil and AO molecules, Fig. 7 presents the C–C bond fracture status of $C_{40}H_{82}$ molecules and the bonding ratio (B_{ab}) of AO molecules of different systems. It should be emphasized that Fig. 7 only presents the bonding ratios that changed, while those that remained constant are treated as unbroken bonds. The bonding ratio is calculated according to the following formula[25]:

$$B_{ab} = \frac{N^t_{ab}}{N^0_{ab}} \tag{2}$$

where N^t_{ab} and N^0_{ab} represent the total number of bonds between atoms a and b at sliding times t and 0 ps, respectively. In AO molecules, a and b range from C2 atoms to C3 and C4 atoms. Since the fracture of $C_{40}H_{82}$ and AO molecules primarily occurs under high-pressure conditions, bonding ratios are calculated only at the end of Stage I (500 ps) and the beginning of Stage III (800 ps).

The fractures in the PAO molecule mainly occur along their main chains, while the introduction of AO reduces the fractures of the main chain, indicating that the protective effect of AO can help base oil resist chain breakage under high-pressure conditions. Different AO molecules exhibit distinct fracture sites, reflecting their varying chemical responses to high-pressure and frictional environments. For C_5H_{10} and $C_{12}H_{24}$ molecules, the decrease in bonding ratio is mainly concentrated at B_{33} (C3-C3 bonds) and B_{44} (C4-C4 bonds), indicating that the breakage of the carbon chain skeleton primarily occurs at the $–CH_2-CH_2-$ and $–CH=CH_2$ sites. The presence of double bonds makes these positions more prone to breakage under high pressure. In contrast, for C_8H_{16} molecules, the decrease in bonding ratios occurs at B_{23} (C2-C3 bonds), B_{33} (C3-C3 bonds), and B_{34} (C3-C4 bonds), corresponding to fractures at the $–CH_3-CH_2-$, $–CH_2-CH_2-$, and $–CH_2-CH=$. Notably, the B_{44} ratio of the $C_{12}H_{24}$ molecule decreases the most significantly, indicating that the breakage mainly occurs at the double-bond site. This observation is consistent with the findings reported by Lai[42]. Although the breakage of this double-bond site is detrimental to the overall stability of the molecular structure, it helps to passivate the dangling bonds on the a-C surface at the friction interface, thereby influencing the tribological performance of the systems.

Before analyzing the hybrid structural changes at the friction interface, it is essential to identify the atoms or molecular fragments in base oil and AO molecules that are prone to chemical bonding with a-C surfaces. This is of great significance for understanding the essence of tribochemical reactions and optimizing lubricating oil molecular design.

Fig. 8 shows the coordination number contribution of base oil and AO to a-C at the end of sliding. When only the base oil is present in the lubricant, C–C bonding often occurs between the upper and lower a-C layers, hindering the sliding process at the interface. However, with the introduction of AO molecules, even after the friction process under high pressure conditions, the lubricant can effectively isolate the upper and lower layers a-C, keeping them in a separated state, which is consistent with the observation results in the morphology graph. This indicates that AO molecules can reduce friction by reducing interfacial C–C cross-linking.

Fig.S3 shows the variation in hybrid structures with sliding times of

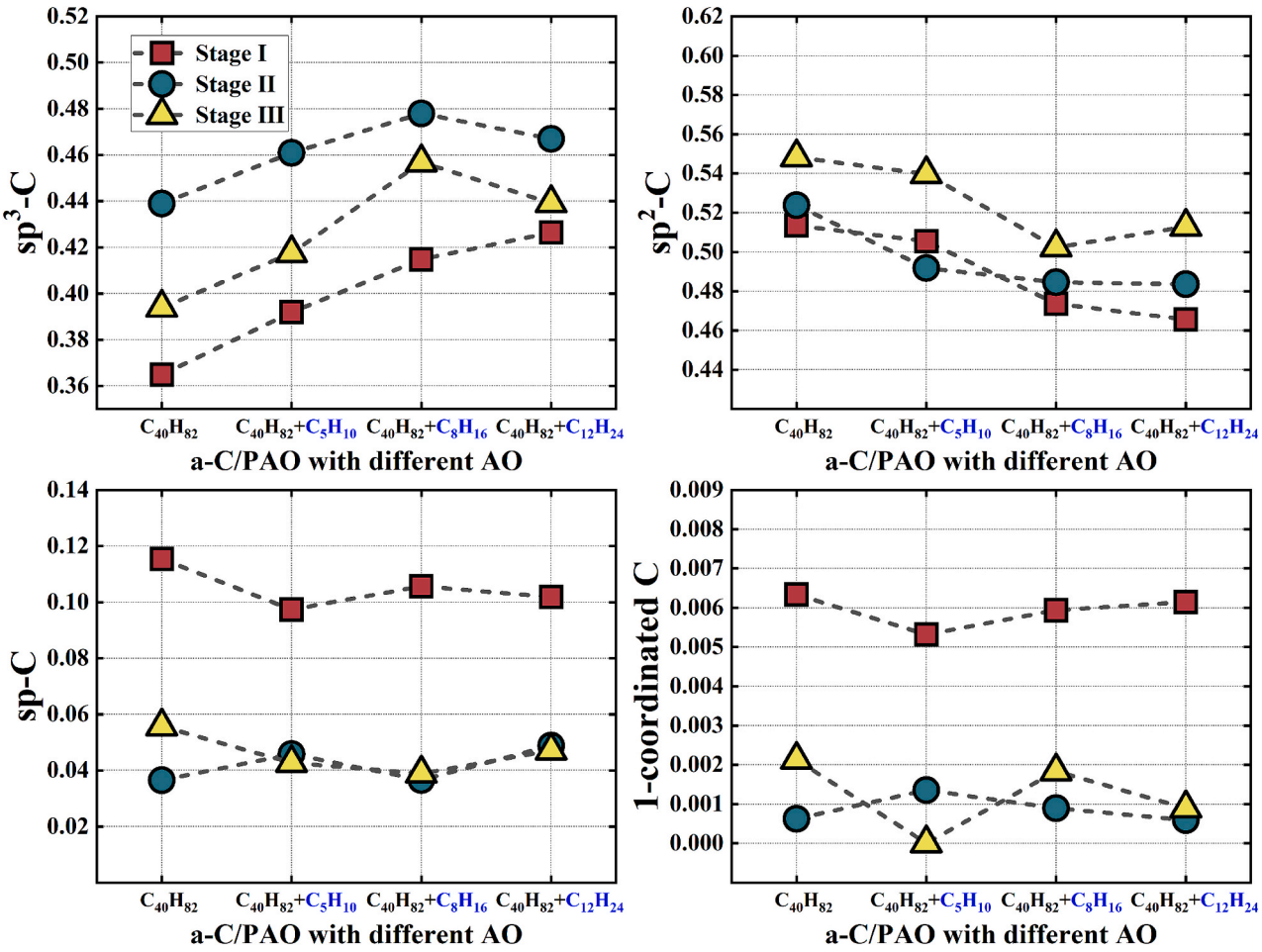

Fig. 9. Hybridization structure of a-C at the interface.

different systems. Noting that the fracture of base oil and AO molecules will affect the hybrid structure of a-C. Therefore, the calculation of the friction interface hybrid structure in this study considers contributions from both a-C and lubricant molecules. For the a-C/$C_{40}H_{82}$/a-C system, during Stage I, as the sliding time increases, the sp^2 carbon content gradually increases due to shear-induced effects, while the sp^3 and sp carbon contents decrease correspondingly. When the pressure rises from 5 GPa to 50 GPa, the sp^3 carbon content increases sharply, indicating significant sp^2-to-sp^3 and sp-to-sp^3 transformations. This phenomenon is closely related to the fractures of lubricant molecules, C–C bondings between the upper and lower a-C, and intensified tribochemical reactions at the interface. At Stage III, as the pressure decreases, some C–C covalent bonds formed between the upper and lower a-C under high pressure partially break, leading to a decrease in sp^3 carbon content and a corresponding increase in sp^2 carbon content during the unloading process. However, the passivation effect of hydrocarbon molecules caused by high-pressure processes results in sp^3 hybridization higher than that of Stage I. This suggests that even a brief high-pressure sliding process can effectively promote the passivation of a-C surfaces, improving tribological performance.

After the introduction of AO, the hybrid structure evolution of the systems is similar to that of the a-C/$C_{40}H_{82}$/a-C system, but the degree of variation differs across stages. Fig. 9 compares the hybrid carbon content of different systems at each stage to quantify these differences more clearly. At Stage I, the increasing chain length of AO molecules leads to a proportional rise in saturated carbon content. However, under high pressure, the fracture of AO molecules and base oil, as well as re-bonding with dangling bonds on the a-C surface, weakens this positive correlation. Consequently, at Stages II and III, the saturated carbon content first increases and then decreases as the chain length of AO molecules grows. This stage-specific variation indicates that AO can significantly optimize the conditions for tribological chemical reactions at the interface as lubricant additives. By selecting AO with appropriate chain lengths, the frictional performance under variable loading conditions can be further improved.

Fig. 10a illustrates the evolution of lubricant fluidity, characterized by mean square displacement (MSD) profiles across different stages and diffusion coefficients calculated from the final 200 ps data, calculated by the following formula[38]:

$$MSD = r^2(t) = \frac{1}{N}\sum |r_i(t) - r_i(0)|^2 = 6Dt$$

where N, $r_i(t)$ and $r_i(0)$ are the number of i atoms in the system, the positions of the i^{th} atom at time t and 0, respectively; D and t represent the diffusion coefficient and sliding time separately.

During stages I and II, the incorporation of AO molecules significantly enhanced lubricant mobility. However, this enhancement exhibited an inverse correlation with AO chain length. These observations indicated that short-chain AO molecules effectively improved lubricant fluidity under both low and high-pressure conditions, whereas the inherent viscosity of long-chain AO molecules constrained their mobility advantages. Conversely, in stage III, the lubricant system demonstrated restored fluidity, with pressure-induced hydrocarbon fragments contributing to enhanced molecular mobility, as evidenced by substantially increased diffusion coefficients. Notably, the presence of AO molecules exhibited a slight inhibitory effect on lubricant fluidity during this stage.

Under low-pressure conditions (Stage I, 5 GPa), enhanced diffusion

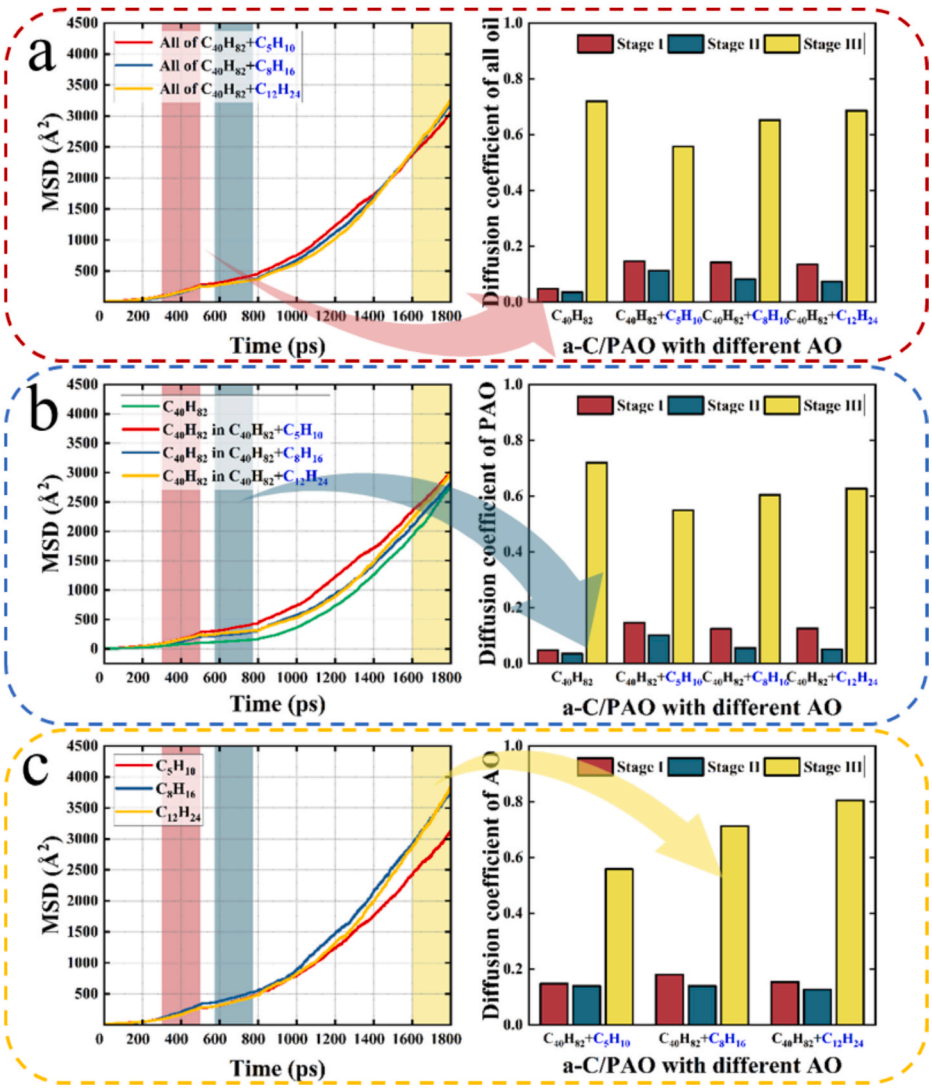

Fig. 10. MSD curves and diffusion coefficient of a) whole lubricant, b) $C_{40}H_{82}$ in each system, and c) only AO in a-C/PAO + AO/a-C systems.

coefficients facilitate hydrodynamic lubrication by promoting lubricant film formation, thereby reducing friction. However, longer-chain AO additives exhibit reduced mobility due to intermolecular van der Waals interactions, leading to higher friction. At extreme pressure (Stage II, 50 GPa), the collapse of diffusion coefficients signifies lubricant film breakdown, transitioning to boundary lubrication dominated by tribochemical passivation and C–C cross-linking. Upon pressure release (Stage III, 5 GPa), partial recovery of diffusion coincides with stabilized friction, where residual passivation layers mitigate direct interfacial contact despite reduced lubricant mobility.

Comprehensive analyses of morphological changes, friction interfacial structure evolution, and lubricant molecular structure and fluidity under varying loading conditions reveal distinct mechanisms by which AO affects tribological performance at different stages:

a) In Stage I, due to the low applied pressure (5 GPa), the lubricant can fully isolate the upper and lower a-C surfaces, with friction behavior dominated by hydrodynamic lubrication, following a relatively low friction coefficient. The introduction of AO enhances lubricant fluidity significantly, but this improvement diminishes with increasing AO chain length, leading to an increase in the friction coefficient with longer AO chains.
b) In Stage II, when pressure increases to 50 GPa, strong chemical interactions occur at the friction interface, with significant cross-linking between the upper and lower a-C layers hindering sliding. Concurrently, base oil and AO molecules fracture into hydrocarbon fragments that passivate intrinsic a-C. Therefore, the competition between C–C bonding and passivation effects under high pressure determines friction behavior, with a significant increase in the friction coefficient. The introduction of AO enhances passivation effects, and variations in saturated carbon hybridization ratios with AO chain length result in slight differences in the friction coefficient.
c) In Stage III, as pressure decreases back to 5 GPa again, long-chain AO molecules fracture into shorter hydrocarbon fragments, reducing differences in tribological performance across systems. Furthermore, the passivation established in Stage II and the elimination of cross-linking between the upper and lower a-C layers significantly reduce the friction coefficient.

As demonstrated in this study, AO molecules exhibit significant potential for integration into PAO-based engine oils and industrial lubricants under variable loading conditions. Under transient high-pressure scenarios (e.g., asperity contacts in engines or gears), AO molecules fragment into hydrocarbon radicals that chemically passivate dangling bonds on a-C surfaces, thereby reducing friction. This mechanism parallels the function of traditional EP additives like ZDDP[43], while eliminating controversial sulfur/phosphorus emissions from an environmental perspective. Furthermore, AO demonstrates dynamic load-

adaptive behavior: under low-pressure (hydrodynamic) conditions, short-chain AO enhances base oil fluidity to improve lubrication efficiency; whereas under sudden high-load (boundary) conditions, long-chain AO preferentially cleaves at double-bond sites to form passivation layers that prevent direct a-C adhesion.

4. Conclusion

This study explored the role of AO as a lubricant additive at the friction interface within the a-C/PAO solid–liquid composite system. Through RMD simulations employing the ReaxFF force field, we systematically investigated the influence of AO on tribological behavior under variable load conditions. Comprehensive analyses were performed to elucidate the molecular interactions between AO (different chain lengths, C_5H_{10}, C_8H_{16}, and $C_{12}H_{24}$), PAO ($C_{40}H_{82}$), and a-C surfaces, along with the evolution of interfacial morphology, structural transformations, lubricant mobility, and friction coefficients. Based on these detailed analyses, the following key findings were established:

- The introduction of AO into the base oil can significantly reduce the friction coefficient. After high-pressure variable loading over a period, the a-C/$C_{40}H_{82}$ + C_8H_{16}/a-C system has the lowest friction coefficient of 0.0314.
- Increasing contact pressure leads to the fracturing of the main chains of base oil molecules. Significantly, AO molecules with extended chain lengths demonstrated superior protective efficacy against molecular fragmentation. The specific fracture sites differ among AO molecules. Notably, the –CH=CH_2 site on the carbon chain skeleton of $C_{12}H_{24}$ molecules exhibits the highest frequency of fractures, suggesting that the primary fracture events in these molecules occur at the double bond.
- The in-depth friction information of system under variable load condition (5–50-5 GPa) is explored. Stage I (5 GPa): The tribological behavior of the investigated systems was predominantly controlled by hydrodynamic lubrication mechanisms. While the incorporation of AO enhanced lubricant fluidity, a progressive increase in AO chain length resulted in elevated friction coefficients, suggesting a chain length-dependent friction response. Stage II (from 5 to 50 GPa): Intensive interfacial interactions between opposing a-C layers resulted in substantial cross-linking phenomena, consequently impeding the sliding process. The decomposed lubricant molecules exhibited beneficial passivation effects on tribological behavior. The addition of AO molecules enhanced these passivation mechanisms, while variations in the distribution of saturated carbon hybridization states induced slight changes in friction coefficients. Stage III (from 50 to 5 GPa): The residual passivation effects from Stage II, coupled with the termination of interfacial bonding between a-C layers, resulted in a reduction in friction coefficients. However, the decomposition of long-chain AO molecules into shorter hydrocarbon fragments weakened the differences in tribological performance across the systems.
- This study provides insights into the friction mechanisms facilitated by AO additives under variable load conditions, presenting a robust theoretical basis for the design and optimization of advanced lubricant formulations. Additionally, these results facilitate the advancement of a-C/fluid lubricant composite systems in mechanical systems subjected to variable loading conditions, thereby promoting their broad application and development in practical engineering scenarios.

CRediT authorship contribution statement

Jiahao Dong: Conceptualization, Data curation, Formal analysis, Investigation, Methodology, Visualization, Writing – original draft. **Naizhou Du:** Formal analysis, Investigation, Methodology, Writing – original draft. **Xubing Wei:** Formal analysis, Investigation, Methodology, Writing – original draft. **Xiang Ji:** Conceptualization, Data curation, Funding acquisition, Investigation, Resources, Supervision, Writing – original draft, Writing – review & editing. **Xuanru Ren:** Formal analysis, Writing – original draft. **Peng Guo:** Formal analysis, Writing – original draft. **Rende Chen:** Formal analysis, Writing – original draft. **Jie Wu:** Formal analysis, Writing – original draft. **Lei Wang:** Formal analysis, Writing – original draft. **Haibin He:** Formal analysis, Writing – original draft. **Kwang-Ryeol Lee:** Formal analysis, Writing – original draft. **Aiying Wang:** Conceptualization, Data curation, Funding acquisition, Investigation, Resources, Supervision, Writing – review & editing. **Xiaowei Li:** Conceptualization, Data curation, Funding acquisition, Investigation, Resources, Supervision, Writing – review & editing.

Declaration of competing interest

The authors declare that they have no known competing financial interests or personal relationships that could have appeared to influence the work reported in this paper.

Acknowledgments

This research was supported by the National Natural Science Foundation of China (No. U24A2030, No. 52175204), Ningbo Science and Technology 2035 Innovation Project (No. 2024Z134), and Joint Fund of Henan Province Science and Technology R&D Program (No. 235200810095).

Appendix A. Supplementary data

Supplementary data to this article can be found online at https://doi.org/10.1016/j.apsusc.2025.163383.

Data availability

Data will be made available on request.

References

[1] K. Holmberg, A. Erdemir, Influence of tribology on global energy consumption, costs and emissions, Friction 5 (2017) 263–284.
[2] Z. Chen, J. Wu, B. Su, Y. Wang, Temperature-structure-induced metastable structural transformation mechanism of the amorphous carbon film during friction, Tribol. Int. 191 (2024) 109112.
[3] Y. Su, Y. Ma, W. Huang, T. Zhang, W. Yu, R. Hu, H. Ruan, The effects of medium and friction pair on the tribological behavior of Mo-doped DLC films, Diam. Relat. Mat. 148 (2024) 111464.
[4] A. Vahidi, F. Ferreira, J. Oliveira, Comparative study of dry high-temperature tribological performance of hydrogen-free and hydrogenated DLC films deposited by HiPIMS in DOMS mode, Tribol. Int. 195 (2024) 109639.
[5] J.G.Z. Tamayo, M. Bjorling, Y. Shi, J. Hardell, R. Larsson, Micropitting performance and friction behaviour of DLC coated bearing steel surfaces: On the influence of Glycerol-based lubricants, Tribol. Int. 196 (2024) 109674.
[6] G. Yang, L. Xu, D. Li, N. Li, G. Zhang, Study on the Lubrication Mechanism of Diamond-Like Carbon Coating in Two Formulated Lubricants with Two Viscosity Grades, J. of Materi Eng and Perform 31 (2022) 6711–6721.
[7] J. Ding, N. Du, X. Wei, X. Li, Z. Chen, S. Lu, H. Zhang, C. Feng, K. Chen, J. Qiao, D. Zhang, K.-R. Lee, Insights into friction behavior of textured amorphous carbon and lubricant composite system: Dependence on the lubricant viscosity and textured shape, Prog. Nat. Sci.: Mater. Int. 33 (2023) 616–624.
[8] X. Li, X. Xu, J. Qi, D. Zhang, A. Wang, K.-R. Lee, Insights into Superlow Friction and Instability of Hydrogenated Amorphous Carbon/Fluid Nanocomposite Interface, ACS Appl. Mater. Interfaces 13 (2021) 35173–35186.
[9] Y. Zhang, H. Chen, K. Gao, Y. Li, J. Jiao, G. Xie, J. Luo, Macroscale Superlubricity with High Pressure Enabled by Partially Oxidized Violet Phosphorus for Engineering Steel, Adv. Funct. Mater. 34 (2024) 2401143.
[10] D. Matsukawa, J.-H. Park, W.-Y. Lee, T. Tokoroyama, J.-I. Kim, R. Ichino, N. Umehara, Tribocatalytic Reaction Enabled by TiO_2 Nanoparticle for MoDTC-Derived Tribofilm Formation at ta-C/Steel Contact, Coatings 14 (2024) 773.
[11] N. Hashizume, Y. Yamamoto, C. Chen, T. Tokoroyama, R. Zhang, D. Diao, N. Umehara, The Effect of Carbon Structure of DLC Coatings on Friction Characteristics of MoDTC-Derived Tribofilm by Using an In Situ Reflectance Spectroscopy, Tribol Lett 72 (2024) 30.

[12] N. Hashizume, M. Murashima, N. Umehara, T. Tokoroyama, W.-Y. Lee, In situ observation of the formation of MoDTC-derived tribofilm on a ta-C coating using reflectance spectroscopy and its effects on friction, Tribol. Int. 162 (2021) 107128.
[13] A. Macknojia, A. Ayyagari, D. Zambrano, A. Rosenkranz, E. Shevchenko, D. Berman, Macroscale Superlubricity Induced by MXene/MoS_2 Nanocomposites on Rough Steel Surfaces under High Contact Stresses, ACS Nano 17 (2023) 2421–2430.
[14] S.-M. Bae, S. Horibata, Y. Miyauchi, J. Choi, Tribochemical investigation of Cr-doped diamond-like carbon with a MoDTC-containing engine oil under boundary lubricated condition, Tribol. Int. 188 (2023) 108849.
[15] L. Čoga, S. Akbari, J. Kovač, M. Kalin, Differences in nano-topography and tribochemistry of ZDDP tribofilms from variations in contact configuration with steel and DLC surfaces, Friction 10 (2022) 296–315.
[16] K. Bobzin, T. Brögelmann, C. Kalscheuer, M. Thiex, Formation mechanisms of zinc, molybdenum, sulfur and phosphorus containing reaction layers on a diamond-like carbon (DLC) coating, Materialwissenschaft Werkst 51 (2020) 1009–1030.
[17] M.M.B. Mustafa, N. Umehara, T. Tokoroyama, M. Murashima, Y. Utsumi, H. Moriguchi, A. Shibata, Effect of PAO-4 and MoDTC plus ZnDTP oil additive lubricants on the tribological performance of novel tetrahedral amorphous carbon (ta-C) coatings, Tribol. Int. 193 (2024) 109396.
[18] [18] V.R.S. Ruiz, T. Kuwahara, J. Galipaud, K. Masenelli-Varlot, M. Ben Hassine, C. Heau, M. Stoll, L. Mayrhofer, G. Moras, J.M. Martin, M. Moseler, M.-I. de B. Bouchet, Interplay of mechanics and chemistry governs wear of diamond-like carbon coatings interacting with ZDDP-additivated lubricants, Nat. Commun. 12 (2021) 4550.
[19] T. Tokoroyama, K. Tanaka, T. Kani, M. Murashima, W.-Y. Lee, N. Umehara, T. Oshio, K. Yagishita, The Tribological Property of a-C:H Coating with Tribolayer by Additive Having Glycerol and Phosphate Oxide Structure, Tribol Lett 70 (2022) 118.
[20] H.A. Tasdemir, M. Wakayama, T. Tokoroyama, H. Kousaka, N. Umehara, Y. Mabuchi, T. Higuchi, The effect of oil temperature and additive concentration on the wear of non-hydrogenated DLC coating, Tribol. Int. 77 (2014) 65–71.
[21] K. Liu, J. Kang, G. Zhang, Z. Lu, W. Yue, Effect of temperature and mating pair on tribological properties of DLC and GLC coatings under high pressure lubricated by MoDTC and ZDDP, Friction 9 (2021) 1390–1405.
[22] H. Okubo, C. Tadokoro, T. Sumi, N. Tanaka, S. Sasaki, Wear acceleration mechanism of diamond-like carbon (DLC) films lubricated with MoDTC solution: Roles of tribofilm formation and structural transformation in wear acceleration of DLC films lubricated with MoDTC solution, Tribol. Int. 133 (2019) 271–287.
[23] T. Tokoroyama, S. Wang, N. Umehara, M. Murashima, W.-Y. Lee, The ta-C Hardness Effect on Wear Properties Under MoDTC Contained Boundary Lubrication, Tribol Lett 72 (2024) 3.
[24] X. Li, A. Wang, K.-R. Lee, Mechanism of contact pressure-induced friction at the amorphous carbon/alpha olefin interface, Npj Comput. Mater. 4 (2018) 53.
[25] X. Li, A. Wang, K. Lee, Tribo-Induced Structural Transformation and Lubricant Dissociation at Amorphous Carbon–Alpha Olefin Interface, Advcd Theory and Sims 2 (2019) 1800157.
[26] M. Ueda, A. Kadiric, H. Spikes, Wear of hydrogenated DLC in MoDTC-containing oils, Wear 474–475 (2021) 203869.
[27] X. Yi, H. Xu, G. Jin, Y. Lu, B. Chen, S. Xu, J. Shi, X. Fan, Boundary slip and lubrication mechanisms of organic friction modifiers with effect of surface moisture, Friction 12 (2024) 1483–1498.
[28] S. Plimpton, Fast Parallel Algorithms for Short-Range Molecular Dynamics, J. Comput. Phys. 117 (1995) 1–19.
[29] X. Li, P. Ke, H. Zheng, A. Wang, Structural properties and growth evolution of diamond-like carbon films with different incident energies: A molecular dynamics study, Appl. Surf. Sci. 273 (2013) 670–675.
[30] H.J.C. Berendsen, J.P.M. Postma, W.F. Van Gunsteren, A. DiNola, J.R. Haak, Molecular dynamics with coupling to an external bath, J. Chem. Phys. 81 (1984) 3684–3690.
[31] F. Tavazza, T.P. Senftle, C. Zou, C.A. Becker, A.C.T. Van Duin, Molecular Dynamics Investigation of the Effects of Tip–Substrate Interactions during Nanoindentation, J. Phys. Chem. C 119 (2015) 13580–13589.
[32] N. Du, C. Feng, K. Chen, J. Qiao, D. Zhang, X. Li, Friction dependence on the textured structure of an amorphous carbon surface: A reactive molecular dynamics study, Appl. Surf. Sci. 610 (2023) 155584.
[33] X. Wei, N. Du, P. Guo, R. Chen, J. Wu, L. Wang, K.-R. Lee, X. Li, H. He, Friction dependence on processing priority for graphitization/passivation coupled amorphous carbon films, Carbon 230 (2024) 119631.
[34] S. Lu, N. Du, X. Li, X. Wei, Z. Chen, J. Ding, C. Feng, K. Chen, J. Qiao, D. Zhang, W. Zhang, Exploring the role of surface hydrogenation in anti-friction of circular-textured amorphous carbon film from the atomic level and its dependence on textured shape, Surf. Interfaces 43 (2023) 103528.
[35] T. Ma, Y. Hu, H. Wang, Molecular dynamics simulation of shear-induced graphitization of amorphous carbon films, Carbon 47 (2009) 1953–1957.
[36] T. Ma, L. Wang, Y. Hu, X. Li, H. Wang, A shear localization mechanism for lubricity of amorphous carbon materials, Sci Rep 4 (2014) 3662.
[37] Z. Chen, N. Du, X. Li, X. Wei, J. Ding, S. Lu, S. Du, C. Feng, K. Chen, D. Zhang, K.-R. Lee, Atomic-Scale Understanding on the Tribological Behavior of Amorphous Carbon Films under Different Contact Pressures and Surface Textured Shapes, Materials 16 (2023) 6108.
[38] N. Du, X. Wei, X. Li, Z. Chen, S. Lu, J. Ding, C. Feng, K. Chen, J. Qiao, D. Zhang, K.-R. Lee, T. Zhang, Friction reactions induced by selective hydrogenation of textured surface under lubricant conditions, Friction 12 (2024) 174–184.
[39] J. Bonaventure, J. Cayer-Barrioz, D. Mazuyer, Surface Effects on Boundary Friction with Additive-Free Lubricating Films: Coupled Influence of Roughness and Material Properties, Tribol. Lett. 66 (2018) 84.
[40] J. Kogovsek, M. Kalin, Comparison of graphene as an oil additive with conventional automotive additives for the lubrication of steel and DLC-coated surfaces, Tribol. Int. 180 (2023) 108220.
[41] N. Du, X. Li, X. Wei, Z. Chen, S. Lu, J. Ding, C. Feng, K. Chen, J. Qiao, D. Zhang, K.-R. Lee, Atomistic Insights into Interfacial Optimization Mechanism for Achieving Ultralow-Friction Amorphous Carbon Films under Solid-Liquid Composite Conditions, ACS Appl. Mater. Interfaces 15 (2023) 53122–53135.
[42] Z. Lai, C. Bai, L. Sun, Q. Jia, K. Gao, B. Zhang, Tribology Dependence of Annealed a-C:H Films in Dry Air and Methanol Environments, ACS Omega 7 (2022) 7472–7480.
[43] S. Zhang, L. Zhu, Y. Wang, J. Kang, H. Wang, G. Ma, H. Huang, G. Zhang, W. Yue, Effects of annealing treatment on tribological behavior of tungsten-doped diamond-like carbon film under lubrication (Part 2): Tribological behavior under MoDTC lubrication, Friction 10 (2022) 1061–1077.